

Ordered particle flow spontaneously generated from random thermal motion

Yu Qiao,^{1,2,*} Zhaoru Shang¹

¹ *Program of Materials Science and Engineering, University of California – San Diego, La Jolla, CA 92093, U.S.A.*

² *Department of Structural Engineering, University of California – San Diego, La Jolla, CA 92093-0085, U.S.A.*

* Email: yqiao@ucsd.edu

Abstract: The second law of thermodynamics is a fundamental pillar in physics. In the current research, we show that it can be broken by a spontaneously nonequilibrium dimension (SND), wherein particle collision is negligible. The SND under investigation is a narrow energy barrier, with the width much less than the particle mean free path. The steady-state particle distribution across the SND is intrinsically in a non-Boltzmann form, causing an ordered particle flow from random thermal motion. When the system is isolated, entropy can decrease; if the system is in a thermal bath, useful work may be produced continuously or cyclically through heat absorption. As the concept is applied to a Fermi gas, a high specific power is predicted.

1. Introduction

For more than a century, the second law of thermodynamics has been critical to many areas in physics, such as energy science and engineering, quantum mechanics, astrophysics, heat and mass transfer, to name a few [1]. However, unlike the first law of thermodynamics (conservation of energy) that is entailed by Noether's theorem [2], the second law of thermodynamics does not have a solid proof. In the elegant H-theorem [3], Boltzmann mathematically constructed the principle of maximum entropy, but the derivation was based on the key assumption of molecular chaos. If the system state is dominated by a process with little particle-particle interaction, no decisive conclusion has been reached.

Over the years, there were continued efforts to analyze the “counterexamples” of the second law of thermodynamics. They have hitherto demonstrated the robustness of the theory of statistical mechanics. In general, these works can be represented by two classical models: Maxwell’s demon [4,5] and Feynman’s ratchet [6]. Both of them have a variety of variants. For example, Maxwell’s demon can operate the Szilárd engine [7]; Feynman’s ratchet is somewhat equivalent to Smoluchowski’s trapdoor [8] and the “autonomous Maxwell’s demon” (i.e., the single-electron refrigerator) [9]. Maxwell’s demon is nonequilibrium, but not spontaneous; Feynman’s ratchet is spontaneous, but not nonequilibrium. Maxwell’s demon relies on external intervention to control the particle behavior and therefore, is subject to the energetic penalty associated with the physical nature of information [10,11]; in Feynman’s ratchet, the time-average behaviors of its components are balanced.

Recently, we investigated the concept of spontaneously nonequilibrium dimension (SND), and showed that a SND-based system might not obey the second law of thermodynamics [12,13]. One example of SND is a narrow barrier with the width much less than the particle mean free path, so that particle-particle collision is negligible inside the SND. Across the SND, the particle distribution cannot reach thermodynamic equilibrium. It combines the nonequilibrium characteristic of Maxwell’s demon with the spontaneity of Feynman’s ratchet. Our first model system employed an energy-barrier SND [12]. The theoretical analysis and the numerical result suggested that useful work could be produced in a cycle by absorbing heat from a single thermal reservoir, which was attributed to the asymmetry in the cross-influence of the thermally correlated thermodynamic forces. Motivated by this finding, we designed and carried out an experiment on an entropy-barrier SND [13]. The testing data demonstrated entropy decrease without energetic penalty. To adapt to these remarkable phenomena and also remain consistent with the principle of maximum entropy, the second law of thermodynamics was generalized as $S \rightarrow S_Q$ [13], i.e., in an isolated system, entropy (S) cannot evolve away from the maximum possible value of steady state (S_Q). When S_Q is equal to the global maximum at thermodynamic equilibrium (S_{eq}), $S \rightarrow S_Q$ is equivalent to the traditional entropy statement, that is, entropy of an isolated system can never decrease. When the boundary condition is changed by the SND, S_Q is reduced, so that S could decrease with it.

The previous model systems in [12] is relatively complicated. The parameters must be alternately adjusted, imposing difficulties to find close analogs in nature or in other fields of physics. The intrinsic energy density is low. The current research is focused on a much-simplified design. Its primary procedure is autonomous.

2. Model System Partly Inspired by Feynman's Ratchet

2.1 Consideration on Feynman's ratchet

Feynman's ratchet is two-ended [6]. One end is a set of vanes, and the other end is a set of ratchet and pawl. They are connected by a rigid rod. Due to the random impacts of the surrounding gas molecules, the vanes undergo a rotational Brownian movement. It seems that the ratchet might selectively guide the oscillation steps, so that the vanes are only allowed to rotate in the forward direction. Yet, such a "perpetual motion machine" would not work. To overcome the energy barrier of the pawl (ΔE_p), the probabilities for both of the vanes and the ratchet are governed by the same Boltzmann factor, $e^{-\beta \cdot \Delta E_p}$, where $\beta = 1/(k_B T)$, k_B is the Boltzmann constant, and T is temperature. Thus, the overall motions of the ratchet and the vanes counterbalance each other. Mere geometric asymmetry does not cause any peculiar effect.

It has been well known that without extensive particle collision, a system can reach a nonequilibrium steady state [14,15], which raises an interesting question: In a two-ended system, what would happen if one end tends to reach thermodynamic equilibrium, while the other end does not? Such a structure could be unbalanced.

2.2 Spontaneously nonequilibrium energy barrier

In this section, we discuss a spontaneously nonequilibrium mechanism of elastic particles, which will be the key component in the model system in Section 2.3 below. Figure 1(A) depicts a vertical y-z plane, wherein a large number of billiard-like particles randomly move in a gravitational field (g). The lateral borders (DC and D'C') are open and use periodic boundary condition. The top boundary and the bottom boundary (DD' and CC') are diffusive walls, from

which the reflected particle velocity follows the two-dimensional (2D) Maxwell-Boltzmann distribution: $p(v) = mv/\bar{K} \cdot e^{-mv^2/2\bar{K}}$, with v being the particle velocity, m the particle mass, and $\bar{K} = k_B T$ the average particle kinetic energy in the 2D system.

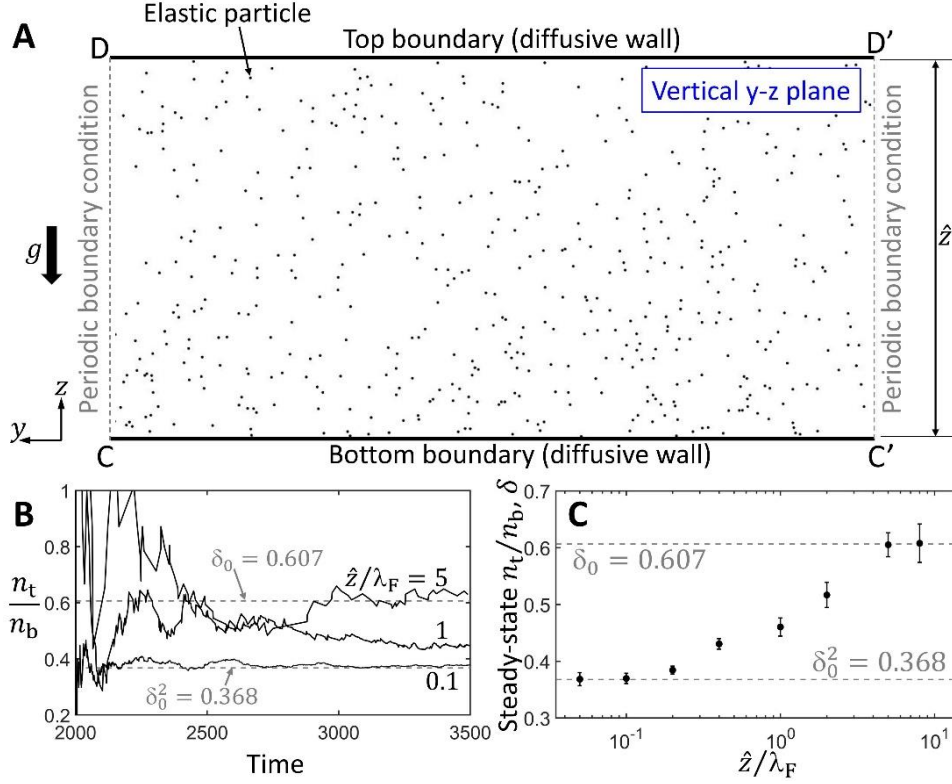


Fig. 1 (A) A vertical plane, in which a large number of elastic particles randomly move in a gravitational field. (B) The results of the Monte Carlo simulation: typical time profiles of the n_t/n_b ratio, and (C) the particle density ratio across the vertical plane (δ) as a function of \hat{z}/λ_F .

Consider a case where the plane height (\hat{z}) is much smaller than the nominal mean free path of the particles, $\lambda_F = A_0/(\sqrt{8}Nd)$, with A_0 being the effective plane area, N the particle number, and d the particle diameter. Under this condition, the particle-particle interaction is negligible, and the system state is dominated by the particle-wall collisions at DD' and CC' . As analyzed in [12], when a particle moves upwards, to overcome the energy barrier of g , the y-component of particle momentum (p_y) has little contribution; only the z-direction kinetic energy ($K_z = mv_z^2/2$) is important, where v_z is the z-component of particle velocity. In general, the particle density ratio across the step can be written as $\delta = \rho_G/\rho_P = e^{-\alpha\beta mg\hat{z}}$ [3], where α is a

location-independent parameter, and ρ_G and ρ_P are the local particle densities near the top boundary ($z = \hat{z}$) and the bottom boundary ($z = 0$), respectively. Since v_z follows the one-dimensional Maxwell-Boltzmann distribution $p_z(v_z) = \sqrt{2m/\pi\bar{K}} \cdot e^{-mv_z^2/2\bar{K}}$, δ can be assessed as $\int_{-\infty}^{\infty} \sqrt{2g\hat{z}} p_z(v_z) dv_z$, which is equal to δ_0^2 , with $\delta_0 = e^{-\beta mg\hat{z}}$ being the Boltzmann factor. It is consistent with the fact that the average K_z is $\bar{K}/2$. Since $\alpha \rightarrow 2$, the steady state is nonequilibrium. Only when $\hat{z}/\lambda_F \gg 1$, with extensive particle-particle collision, would the system approach thermodynamic equilibrium, so that $\alpha \rightarrow 1$.

The influence of \hat{z} on δ is visualized by a Monte Carlo (MC) simulation. The computer program is available at [16]. The setup is scalable; an example of the unit system can be based on K, g/mole, Å, and fs. The particle diameter (d) is 1; $A_0 = \hat{z} \cdot w_0 = 39268.75$, where $\hat{z} = h - d$, and h and w_0 are the height and the width of the simulation box, respectively; $N = 500$; $m = 1$; $T = 300$. It can be calculated that $\lambda_F \approx 27.77$, and the percentage of the occupied area of the particles is $N\pi d^4/(4A_0) \approx 1\%$. In different simulation cases, \hat{z} is varied; \hat{z}/λ_F is 0.05, 0.1, 0.2, 0.4, 1, 2, 5, or 8. The width of the simulation box (w_0) is changed accordingly, to keep A_0 and λ_F constant. The gravitational acceleration (g) is also adjusted to maintain $\beta mg\hat{z} = 0.5$, so that the Boltzmann factor remains the same $\delta_0 = e^{-\beta mg\hat{z}} = 0.607$. At time zero, all the particles are randomly generated. The probability density function of the initial velocity is $p(v)$, and the initial direction is random. If $\hat{z}/\lambda_F < 1$, the timestep of the simulation (Δt_0) is set to 0.0183; if $\hat{z}/\lambda_F \geq 1$, $\Delta t_0 = 0.0058$.

For each simulation case, after the settlement period ($t_{sp} = 1.826 \times 10^3$), we begin to count the numbers of the particle-wall collisions at the top boundary (n_t) and the bottom boundary (n_b). Figure 1(B) shows typical time profiles of the running average of the n_t/n_b ratio. The particle density ratio across the plane (δ) is estimated as the steady-state n_t/n_b . The total simulation time is more than 2×10^5 timesteps, to reach the steady state. Figure 1(C) shows the calculated $\delta - \hat{z}$ relationship. For each \hat{z}/λ_F , three nominally same simulations are carried out, with randomized initial conditions. The error bars are the 90%-confidence interval, $\pm 1.645 \cdot s_t/\sqrt{3}$, with s_t being the standard deviation. The results clearly indicate that when $\hat{z} \gg \lambda_F$ (i.e., when the particle-particle interaction is extensive), $\delta \rightarrow \delta_0$; when $\hat{z} \ll \lambda_F$ (i.e., when the particle-particle interaction is negligible), $\delta \rightarrow \delta_0^2$.

2.3 Model system

Figure 2(A,B) depicts the model system of randomly moving elastic particles. The central area (the upper “plateau”) is higher than the rest of the area (the lower “plain”). The particle movement in the plateau and the plain is ergodic and chaotic. The plateau height is \hat{z} , which is much less than λ_F . A uniform gravitational field (g) is along $-z$, normal to the plain and the plateau. The left-hand side and the right-hand side of the plateau are connected to the plain through a vertical step and a wide ramp, respectively. The ramp size (\hat{L}) is much larger than λ_F .

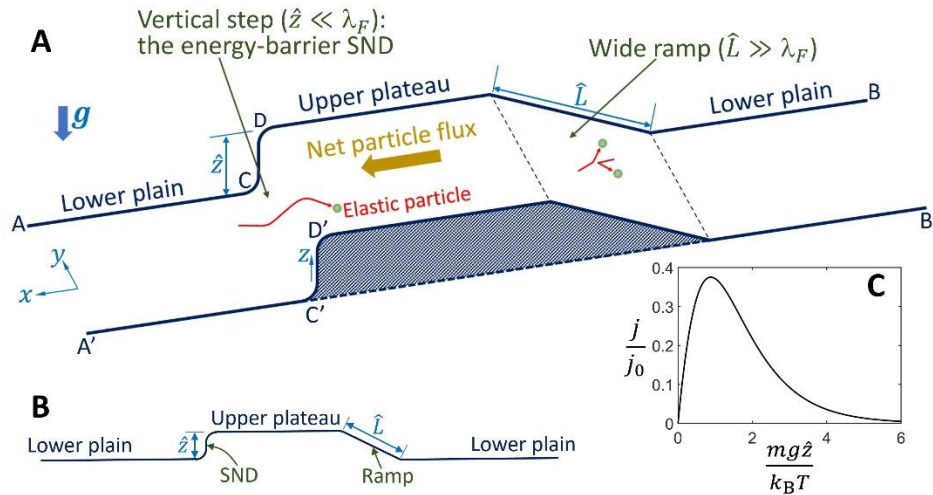


Fig. 2 (A) Three-dimensional view and (B) side view of the step-ramp model system. (C) The particle flux, j , predicted by Equation 1 ($\alpha = 2$ and $\tilde{A} = 1$).

On the one hand, since $\hat{L} \gg \lambda_F$, the particle collision in the ramp is extensive. Across the ramp, to maximize entropy, the particle density ratio between the plateau and the plain tends to be the Boltzmann factor [3], $\delta_0 = e^{-\beta mg\hat{z}}$. On the other hand, as shown in Figure 1(B,C), across the locally nonchaotic vertical step, the particle density ratio (δ) tends to be δ_0^2 . For the sake of simplicity, here we analyze a system in which the plateau and the plain are much larger than the ramp and the step. The average particle densities on the plateau (ρ_G) and the plain (ρ_P) can be assessed through $\rho_G A_G + \rho_P A_P \approx N$ and $\rho_G / \rho_P \approx \bar{\delta}$, where $\bar{\delta} = (\delta_0 + \delta) / 2$, and A_G and A_P are the areas of the plateau and the plain, respectively. Thus, $\rho_P = N / (\bar{\delta} A_G + A_P)$. Because $\delta \neq \delta_0$,

on the plateau, there would be a net particle flux from the high-density area (the ramp side) to the low-density area (the step side):

$$j = \frac{1}{2}(\rho_P \delta_0) \bar{v}_x - \frac{1}{2}(\rho_P \delta) \bar{v}_x = \frac{1}{2} \frac{\tilde{\rho}}{\delta \tilde{A} + 1} \Delta \delta \cdot \bar{v}_x \quad (1)$$

where $\tilde{\rho} = N/A_P$, $\Delta \delta = \delta_0 - \delta$, $\tilde{A} = A_G/A_P$, and $\bar{v}_x = \sqrt{2k_B T / (\pi m)}$. The drift velocity may be estimated as

$$v_w = \frac{j}{\rho_P} = \frac{1}{2} \Delta \delta \cdot \bar{v}_x \quad (2)$$

Figure 2(C) shows one example of Equation (1), where $j_0 = \bar{\rho} \cdot \bar{v}_x / 2$, $\bar{\rho} = N/A_{\text{tot}}$, and A_{tot} is the total system area. When $\hat{z} = 0$, the energy barrier vanishes, so that $j = 0$. When the energy barrier is large, because both δ_0 and δ are small, few particles are on the plateau and consequently, j is also near zero. When $\beta m g \hat{z}$ is in the middle range, j is significant.

3. Monte Carlo Simulation

To demonstrate the concept of Figure 2, we performed a MC simulation on an isolated 2D system. The computer program is available at [16]. The simulation box represents the surface of particle movement (Figure 3A). From left to right, it contains a left plain (“+”), a step, a plateau, a wide ramp, and a right plain (“-”). The left and the right borders (AA' and BB') are open and use periodic boundary condition. The upper and the lower borders (AB and A'B') are rigid specular walls. The simulation is scalable; an example of the unit system can be based on nm, fs, g/mol, and K. The width of the box between AB and A'B' (w_0) is 50. The length of each plain (“+” or “-”) is $L_P = 5$. The plateau length (L_G) is 10. The step size (\hat{z}) is 0.5. The ramp size (\hat{L}) is 50. The total particle number $N = 500$. Temperature $T = 1000$. The particle diameter $d = 0.2$, and $m = 1$. The time step $\Delta t_0 = 1$. The nominal mean free path of the particles is $\lambda_F \approx 12.46$, much larger than \hat{z} while considerably smaller than \hat{L} .

Initially, all the particles are uniformly distributed on the plain. Their velocities follow $p(v)$, and the directions are random. If the total initial x-component of momentum of all the particles is larger than $10^{-3} p_0$, the configuration would be rejected, where $p_0 = \sqrt{2mk_B T / \pi}$. There is no long-range force on the plain and the plateau. In the step surface, from right to left, the gravitational acceleration is denoted by g . In the ramp surface, from left to right, the component

of gravitational acceleration is $\hat{z}g/\hat{L}$. In different simulation cases, g is adjusted, so that $\beta mg\hat{z}$ varies from 0 to 2.

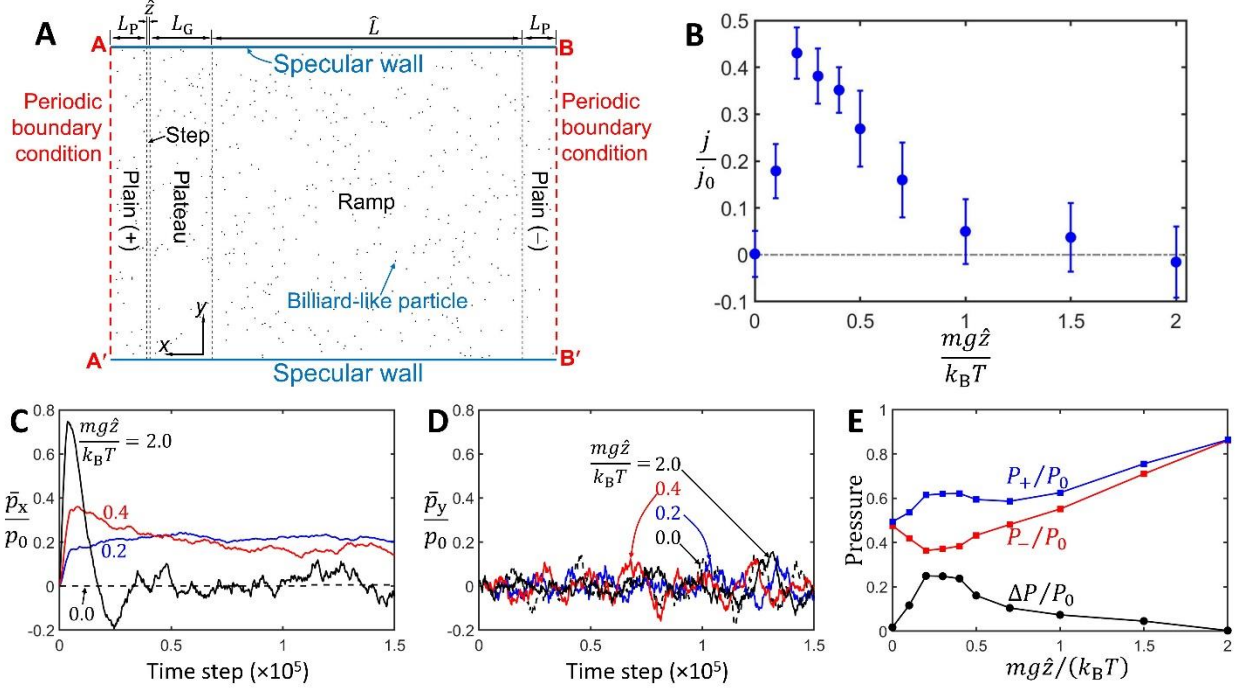


Figure 3 (A) The Monte Carlo simulation. (B) The calculated particle flux (j) as a function of $\beta mg\hat{z}$. (C) Typical time profiles of the average x-component of particle momentum (\bar{p}_x) and (D) the average y-component of particle momentum (\bar{p}_y). (E) The inner pressure at the lateral border (AA' and BB'), where $P_0 = Nk_B T/A_{\text{tot}}$.

Each time when a particle crosses the lateral border (AA' and BB'), the time, the velocity, and the direction are recorded. The particle flux (j) is calculated as $(n_+ - n_-)/(w_0\Delta t)$ for every $\Delta t = 5000$ timesteps (Figure 3B), where n_+ and n_- are the numbers of the crossing events from plain “+” to “-” and from plain “-” to “+”, respectively. The error bars are the 90%-confidence interval, $\pm 1.645 \cdot s_t/\sqrt{n_t}$, where n_t is the number of data points. The average particle momentums are $\bar{p}_x = \frac{1}{N} \sum m v_x$ and $\bar{p}_y = \frac{1}{N} \sum m v_y$, where Σ indicates summation for all the particles, and v_x and v_y are the x-component and the y-component of particle velocity, respectively. The time-average \bar{p}_x and \bar{p}_y are computed for every 200 timesteps (Figure 3C,D). The partial pressure is calculated as $P_{\pm} = \frac{1}{w_0\Delta t} \sum_{\pm} m v_x$, where Σ_+ and Σ_- indicate summation in every 5000 timesteps (Δt) for the

particles crossing the lateral border from plain “+” to “-” and from plain “-” to “+”, respectively. The inner pressure is $\Delta P = P_+ - P_-$ (Figure 3E).

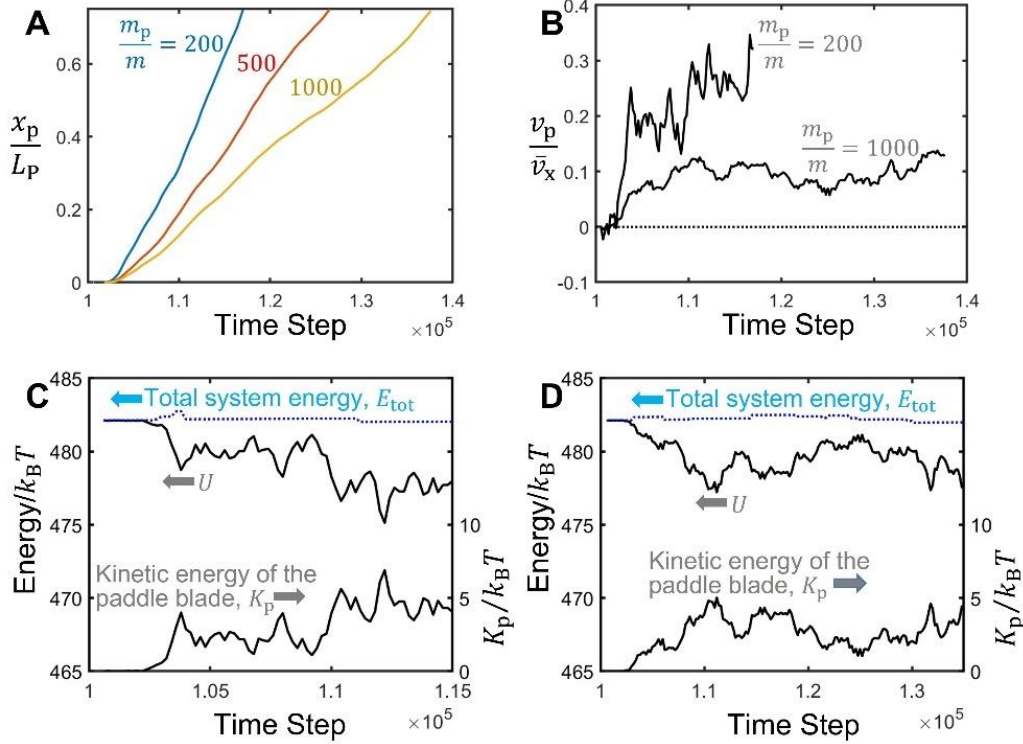


Figure 4 A paddle blade is driven by the particle flux, converting thermal energy to useful work, K_p . (A) Typical time profiles of the displacement (x_p) and (B) the velocity (v_p) of the paddle blade. (C) Typical energy evolution when $m_p = 200m$ and (D) $m_p = 1000m$.

When $\beta mg\hat{z} = 0.2$, after the system reaches the steady state, a paddle blade is placed at the middle of plain “+”. It is modeled as a rigid specular line normal to the x axis, with the length of w_0 and the mass (m_p) of $200m$, $500m$, or $1000m$. It can freely move along the x direction, but does not move along the y direction or rotate. Figure 4(A,B) shows that the paddle blade is driven by the particle flux. When its displacement (x_p) exceeds $0.5L_p$, it crosses the lateral border from plain “+” to “-”. Figure 4(C,D) shows the energy evolution: U is the total kinetic energy and potential energy of all the particles, and the kinetic energy of the paddle blade is $K_p = m_p v_p^2/2$, where v_p is its velocity. The increase in K_p matches the reduction in U . The overall energy, $E_{tot} = U + K_p$, remains constant, as it should.

4. Discussion

4.1 Contradiction to the second law of thermodynamics

Figure 3(B) qualitatively agrees with Figure 2(C). The difference between them should be attributed to the large ramp area, the isolated boundary condition, and the local anisotropy and heterogeneity in the MC simulation. In both figures, when $\beta mg\hat{z}$ is 0.1~1, a relatively large particle flux is observed. This is compatible with Figure 3(C-E). The particle movement along the y direction is unordered, so that \bar{p}_y remains near zero. With the particle flux (j), the steady-state \bar{p}_x is nontrivial. The change in \bar{p}_x comes from the unbalanced reaction forces on the step and the ramp. Due to the biased particle movement, $P_+ > P_-$ and there is a significant inner pressure (ΔP). It serves as the driving force of the paddle blade, converting thermal energy to the useful work, K_p . If the system can exchange heat with the environment (e.g., a thermal bath), the thermal-to-kinetic energy conversion may be operated either continuously or in a cycle.

In Figure 2(A), the system is isolated. The narrow step imposes a set of constraints on the probability of system microstates [13]. Entropy is equal to the global maximum (S_{eq}) when $\bar{\delta} = \delta_0$ and $v_w = 0$, corresponding to thermodynamic equilibrium. If $\bar{\delta} \neq \delta_0$ and $v_w \neq 0$, when S is maximized, it reaches a local maximum (S_{ne}) less than S_{eq} . Assume that the plain size and the plateau size are much larger than the step size and the ramp size, so that $N \approx N_P + N_G$, where N_P and N_G are the particle numbers on the plain and the plateau, respectively. Initially, the system is at thermodynamic equilibrium, and the particle density ratio between the plateau and the plain is the Boltzmann factor. Hence, $N_P = N/(\delta_0\tilde{A} + 1)$ and $N_G = N\delta_0\tilde{A}/(\delta_0\tilde{A} + 1)$. Based on the entropy equation of ideal gas [3], we have

$$S_{\text{eq}} = \frac{N}{\delta_0\tilde{A}+1} k_B \left[\ln \frac{A_P(\delta_0\tilde{A}+1)}{N} + \sigma_0 \right] + \frac{N\delta_0\tilde{A}}{\delta_0\tilde{A}+1} k_B \left[\ln \frac{A_G(\delta_0\tilde{A}+1)}{N\delta_0\tilde{A}} + \sigma_0 \right] \quad (3)$$

where $\sigma_0 = \frac{3}{2} \ln \left(\frac{4\pi e}{3} m k_B T \right)$. The first and the second terms of Equation (3) are the contributions from the plain and the plateau, respectively. When the system is at the nonequilibrium steady state with the net particle flux (j), the system entropy becomes

$$S_{\text{ne}} = \frac{N}{\bar{\delta}\tilde{A}+1} k_B \left[\ln \frac{A_P(\bar{\delta}\tilde{A}+1)}{N} + \sigma \right] + \frac{N\bar{\delta}\tilde{A}}{\bar{\delta}\tilde{A}+1} k_B \left[\ln \frac{A_G(\bar{\delta}\tilde{A}+1)}{N\bar{\delta}\tilde{A}} + \sigma \right] \quad (4)$$

where $\sigma = \frac{3}{2} \ln \left(\frac{4\pi e}{3} m k_B \hat{T} \right)$, and $\hat{T} = T - \frac{mv_w^2}{2k_B}$ is the effective temperature. As the ordered particle flow is generated in the initially unordered system, S is reduced from S_{eq} to S_{ne} . The entropy decrease, $\Delta S = S_{ne} - S_{eq}$, comes from the unforced thermal movement. It is associated with the difference of $\bar{\delta}$ and \hat{T} from δ_0 and T . The former ($\bar{\delta}$) represents the influence of the particle distribution; the latter (\hat{T}) reflects the degree of randomness of particle velocity.

It is worth noting that the system does not consume any energy from the gravitation field, since the steady-state particle flux is continuous. On average, for every particle moving up the ramp, there is a particle moving down the step. The produced work (K_p) is from thermal energy (see Figure 4C,D).

4.2 High specific power in Fermi gas

If the particles are air molecules, at room temperature, \bar{v}_x is ~ 270 m/s. According to Equation (2), the maximum drift velocity is 50~60 m/s, comparable to the wind speed of a Category 5 hurricane. However, to achieve a nontrivial particle flow, g must be greater than 10^{12} m/s², around the level of neutron stars [17].

The energy barrier may be based on Coulomb force, for which the working medium can be a Fermi gas. For instance, in a metal, the Fermi velocity (v_F) is on the scale of 10^6 m/s [18]. The mean free path of the conduction electrons (λ_e) is 40~60 nm [19] and their density (ρ_e) is a few 10^9 C/m³ [18]. If a metallic nanowire or nanolayer has an asymmetric structure with a nano-step at one end and a wide slope at the other end (Figure 5), in an external electric field (E), a diffusive current may be spontaneously generated, analogous to Figure 2(A). The nano-step size (\hat{z}) should be much less than λ_e ; the slope size (\hat{L}) should be much larger than λ_e . Similar to j_0 , the reference current density is $j_{e0} = \rho_e v_F / 2$, on the scale of 10^{15} A/m². Figures 2(C) and 3(B) suggest that the maximum possible current density is a fraction of j_{e0} , on the scale of 10^{14} A/m². For a metallic nanowire 1 μ m in length and 10 nm² in cross section, the resistance is $10^3 \sim 10^4$ Ω , and the maximum current may be ~ 1 mA. Under this condition, the upper limit of the specific power is on the order of 10^{15} W/kg; the associated specific energy can reach the level of nuclear

reactions ($10^7 \sim 10^8$ MJ/kg) in less than 0.1 sec. Multiple nano-steps may be placed in tandem and/or in parallel.

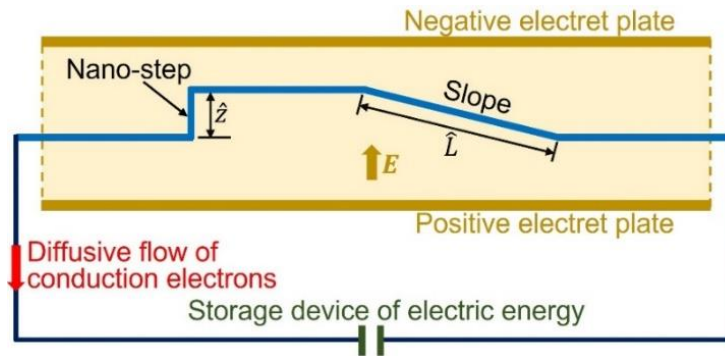


Figure 5. A nonequilibrium nanowire that spontaneously produces electric energy by absorbing heat from the environment (a thermal bath).

4.3 Implications

In addition to gravity and Coulomb force, many other thermodynamic forces are also relevant, including inertial force and magnetic momentum; in addition to the narrow energy barrier, many other geometric or non-geometric mechanisms are also applicable, such as switchable or distributed components [12], entropy barrier [13], etc. An important future research topic is to explore whether similar spontaneous or “perpetual” movements may exist in nature, e.g., on the atomic/subatomic scales, in a high- g environment, or with weak/sparse particle interaction. The system state evolution in phase space must be examined in detail.

5. Concluding Remarks

To summarize, a narrow energy barrier is employed to form a spontaneously nonequilibrium dimension (SND). The system behavior is both spontaneous and nonequilibrium. An ordered particle flow is generated from unforced thermal motion. It leads to entropy decrease in an isolated setup, which also allows for production of useful work in a cycle from a single thermal reservoir. These phenomena cannot be explained in the conventional framework of

statistical mechanics, while are consistent with the generalized second law of thermodynamics ($S \rightarrow S_Q$).

References

1. I. Müller. *A History of Thermodynamics* (Springer, 2007).
2. Y. Kosmann-Schwarzbach. *The Noether Theorems* (Springer, 2010).
3. M. Kardar. *Statistical Physics of Particles* (Cambridge Univ. Press, 2007)
4. H. S. Leff, A. F. Rex. *Maxwell's Demon: Entropy, Information, Computing* (Princeton Univ. Press, 1990)
5. D. V. Averin, M. Möttönen, J. P. Pekola. Maxwell's demon based on a single-electron pump. *Phys. Rev. B* **84**, 245448 (2011).
6. R. P. Feynman, R. B. Leighton, M. Sands. *The Feynman Lecture Notes on Physics*, Vol. 1, Chapt. 46 (Basic Books, 2011)
7. D. Mandal, C. Jarzynski. Work and information processing in a solvable model of Maxwell's demon. *Proc. Natl. Acad. Sci. U.S.A.* **109**, 11641 (2012)
8. P. A. Skordos, W. H. Zurek. Maxwell's demon, rectifiers, and the second law: Computer simulation of Smoluchowski's trapdoor. *Am. J. Phys.* **60**, 876 (1992).
9. J. V. Koski, A. Kutvonen, T. Ala-Nissila, J. P. Pekola. On-chip Maxwell's demon as an information-powered refrigerator. *Phys. Rev. Lett.* **115**, 260602 (2015).
10. R. Landauer. Information is inevitably physical, in *Feynman and Computation*, pp77-92 (Perseus Books, Cambridge, MA, 1998)
11. D. Mandal, C. Jarzynski. Work and information processing in a solvable model of Maxwell's demon. *Proc. Natl. Acad. Sci. U.S.A.* **109**, 11641 (2012)
12. Y. Qiao, Z. Shang. Producing useful work in a cycle by absorbing heat from a single thermal reservoir: An investigation on a locally nonchaotic energy barrier, *Physica A* (2022)
<https://doi.org/10.1016/j.physa.2022.127105>

13. Y. Qiao, Z. Shang, R. Kou. Molecular-sized outward-swinging gate: Experiment and theoretical analysis of a locally nonchaotic barrier. *Phys. Rev. E*, **104**, 064133 (2021)
<https://doi.org/10.1103/PhysRevE.104.064133>
14. G. Lebon, D. Jou. *Understanding Nonequilibrium Thermodynamics* (Springer, 2008)
15. A. Argun, A. Moradi, E. Pince, G. B. Bagci, A. Imparato, G. Volpe. Non-Boltzmann stationary distributions and nonequilibrium relations in active baths. *Phys. Rev. E* **94**, 062150 (2016).
16. Z. Shang, Y. Qiao. The computer programs developed for the current research, available at http://mmrl.ucsd.edu/Z_Upload/Papers/ComputerPrograms_Flux.zip
17. M. Camenzind. *Compact Objects in Astrophysics* (Springer, 2016)
18. R. P. Huebener. *Conductors, Semiconductors, Superconductors* (Springer, 2016)
19. D. Gall. Electron mean free path in elemental metals. *J. Appl. Phys.* **119**, 085101 (2016)